文章编号：1001-9014(2022)01-0269-10

DOI:10. 11972/j. issn. 1001-9014. 2022. 01. 021

# Design of a diagonally symmetrical photonic crystal fiber for chemical sensing

ZHAO Li-Juan[1,2,3], ZHAO Hai-Ying[1], XU Zhi-Niu[4*], LIANG Ruo-Yu[1]

(1. Department of Electronic and Communication Engineering, North China Electric Power University, Baoding 071003, China;
2. Hebei Key Laboratory of Power Internet of Things Technology, North China Electric Power University, Baoding 071003, China;
3. Baoding Key Laboratory of Optical fiber sensing and optical communication Technology, North China Electric Power University, Baoding 071003, China;
4. School of Electrical and Electronic Engineering, North China Electric Power University, Baoding 071003, China)

**Abstract**: A novel photonic crystal fiber with high birefringence and low confinement loss is designed, which can be used for chemical sensing . The effects of air holes parameters on optical properties of optical fiber are systematically investigated. The results reveal that the relative sensitivities of the fiber with the optimal structure for water, ethanol and benzene at the wavelength of 1. 55 μm are 56. 3%, 59. 9% and 62. 5%, respectively. Compared with the existing PCFs, they are improved by 1. 05-6. 25 times, 1. 05-4. 99 times and 1. 03-4. 63 times, respectively. Besides, it has excellent transmission characteristics. Therefore, the proposed photonic crystal fiber has advantages in chemical sensing and biomedicine filed.

**Key words**: photonic crystal fiber, chemical sensing, relative sensitivity, finite element method, high birefringence

# 一种可用于化学传感的对角对称光子晶体光纤设计

赵丽娟[1,2,3], 赵海英[1], 徐志钮[4*], 梁若愚[1]

(1. 华北电力大学,电子与通信工程系,河北 保定 071003;
2. 华北电力大学 河北省电力物联网技术重点实验室,河北 保定 071003;
3. 华北电力大学 保定市光纤传感与光通信技术重点实验室,河北 保定 071003;
4. 华北电力大学,电气与电子工程学院,河北 保定 071003)

**摘要**:本文提出了一种可用于化学传感的具有高双折射、低损耗的光子晶体光纤,并系统地分析了空气孔参数对光纤光学特性的影响。研究表明,最优结构的光纤在典型波长 1.55 μm 时对水、乙醇和苯的相对灵敏度分别可达 56.3%、59.9% 和 62.5%,相比现有光子晶体光纤分别提高 1.05~6.25 倍、1.05~4.99 倍和 1.03~4.63 倍。此外,该光纤还具有较好的传输特性。因此,本文提出的光子晶体光纤在化学传感和生物医学领域方面更具优势。

**关 键 词**:光子晶体光纤;化学传感;相对灵敏度;有限元法;高双折射

## Introduction

Photonic crystal fiber (PCF) has flexible designability of parameters and exhibits excellent properties, which are difficult to achieve for traditional optical fibers. Therefore, it is widely used in monitoring chemical analytes, temperature sensing application and pressure sensor [1-4]. With the development of industry, environmental pollution has attracted more attention, which promoted the development of research on the sensing and monitoring of chemical analytes by the use of PCF. In fact, the sensing mechanism of chemical sensing appli-

**Received date**: 2021- 03- 24, **revised date**: 2021- 10- 29 **收稿日期**:2021- 03- 24,**修回日期**:2021- 10- 29

**Foundation items**: Supported by the National Natural Science Foundation of China ( 61775057, 62171185), the Natural Science Foundation of Hebei Province, China ( E2020502010, E2019502177), the Fundamental Research Funds for the Central Universities ( 2019MS085, 2021MS072), S & T Program of Hebei (SZX2020034).

**Biography**: ZHAO Lijuan (1981-), female, Baoding, associate professor, doctor. Research area involves optical communication and sensing. E-mail: hdzlj@126. com.

[*] **Corresponding author**: E-mail: wzcnjxx@163. com

cation using PCF is based on the interaction between light (evanescent wave) and chemical analytes, then PCF senses the type and concentration of analytes from the action results to monitor the environmental quality and toxic gases.

One obvious way to optimize performance of PCF is designing different structures and improving the asymmetry of the structure, such as introducing air holes with different radii in the cladding or changing the shape of air holes. In 2018, Hou[5] *et al.* proposed a kind of PCF with the birefringence of $2.89\times10^{-2}$ by introducing elliptical air holes. In 2019, Rekha[6] *et al.* designed an axisymmetric PCF with the birefringence up to $2.75\times10^{-2}$ at the wavelength of 1.55 μm, but its confinement loss needs to be improved. At the same time, researchers have generated some significant research on the design of optical fiber to improve the relative sensitivity. For example, in 2016, Ademgil[1] *et al.* achieved the relative sensitivities of 9%, 12% and 13.5% for water, ethanol and benzene respectively by asymmetrically introducing 3 circular air holes in the core of PCF. In 2018, Paul[7] *et al.* presented a slotted core PCF as a gas sensor with the relative sensitivity of 48.26% at the wavelength of 1.33 μm. In 2019, Rabee[8] *et al.* designed a kind of PCF with 5 layers of air holes in the cladding and a spiral arrangement of air holes in the core. They obtained that the relative sensitivity for gas is 72.04% at the wavelength of 1.33 μm. Malavika[9] *et al.* proposed a spiral shaped PCF for liquid sensing application. At the wavelength of 1.55 μm, the relative sensitivities achieved 56.8%, 58.3% and 62.7% for water, propane and propylene respectively, but its confinement loss is above $10^{-7}$ dB/m. In 2020, Kabir[10] *et al.* proposed a PCF structure with hexagonal arrangement for circular air holes, its relative sensitivities for water are 49.13% and 46% at the wavelength of 1.3 μm and 1.55 μm respectively. In 2021, Leon[11] *et al.* designed a PCF with the hexagonal configuration of circular air holes in the cladding, the sensitivity for water is about 40% at the wavelength of 1.55 μm. Although most of the existing works adopting axisymmetric structures have made great progress, PCFs with better transmission characteristics and higher relative sensitivity are often required in practical applications.

Different from the axisymmetric structure used in the existing PCFs, a novel PCF with air holes arranged in a triangular lattice is proposed in this work. The proposed PCF is designed as diagonally symmetrical structure rather than axisymmetric structure, which increases the asymmetry of PCF and improves its properties further. The parameters of optimal structure are obtained through numerical calculation and the comparison with existing PCFs[1-17]. The proposed PCF provides a choice for the applications in the biomedicine filed and chemical sensing applications.

## 1 Structure and theoretical model of the designed fiber

### 1.1 Structure of the designed fiber

The cross-section of the designed PCF is shown in Fig. 1 (In Fig. 1, the air holes with same size have the same color). The air holes in the cladding are arranged in a diagonally symmetrical triangular array. Where, the semi-major axis of ellipse along the $x$-axis is represented by $a_1$, the semi-minor axis of ellipse along the $x$-axis is represented by $b_1$, the distance of the hole is called pitch and it is denoted by $\Lambda_i$, the pitch of this ellipse is $\Lambda_1$=1.4 μm; the semi-major axis of ellipse in a triangular lattice is $a_2$=1 μm, the semi-minor axis of small ellipse in a triangular lattice is $b_2$=0.7 μm, and the pitch of this ellipse is $\Lambda_2$=1 μm; the diameter of large circle is $d_1$=1 μm, the pitch of large circle is $\Lambda_3$=1 μm; the diameter of small circle is $d_2$=0.8 μm, the pitch of small circle is $\Lambda_4$=0.8 μm; the diameter of cladding is 13 μm; and the diameter of Perfectly Matched Layer (PML) is $d$=13.65 μm.

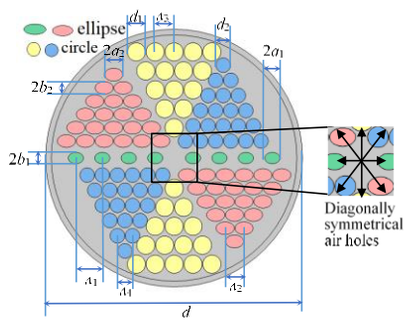


Fig. 1 The cross-section of the designed PCF
图1 本文所设计光子晶体光纤的横截面

The PCF structure is designed as diagonally symmetrical structure and some of these air holes are designed as ellipse to increase the asymmetry of the optical fiber and improve its properties. The details are as follows. Firstly, the diagonally symmetrical structure causes part of the energy to leak into the cladding, which will enhance the interaction between evanescent wave and chemical analytes and increase the relative sensitivity. Note that excessive energy leaking into the cladding will also result in the increase in confinement loss. Secondly, the cladding contains many layers of air holes to decrease the confinement loss and guide as much as possible light through the core. Thirdly, the birefringence ($B$) in PCF is defined as

$$B = \frac{\left|\beta_x - \beta_y\right|}{2\pi/\lambda} = \left|\mathrm{Re}\left(n_{\mathrm{eff}}^x\right) - \mathrm{Re}\left(n_{\mathrm{eff}}^y\right)\right| \quad , \quad (1)$$

where $\lambda$ represents the wavelength, $\beta_x$ and $\beta_y$ represent propagation constants of $x$-pol and $y$-pol, $n_{\mathrm{eff}}^x$ and $n_{\mathrm{eff}}^y$ represent effective refractive index of $x$-pol and $y$-pol, respectively. $\mathrm{Re}\left(n_{\mathrm{eff}}^x\right)$ represents the real component of $n_{\mathrm{eff}}^x$. The introduction of elliptical air holes and the diagonally symmetrical arrangement of cladding contributes to the asymmetry of the structure, making the difference between $\beta_x$ and $\beta_y$ bigger and the birefringence higher.

The background material is $SiO_2$, the refractive index of $SiO_2$ is determined by the following Sellmeier equation.

$$n(\lambda)=\sqrt{1+\frac{B_1\lambda^2}{\lambda^2-C_1}+\frac{B_2\lambda^2}{\lambda^2-C_2}+\frac{B_3\lambda^2}{\lambda^2-C_3}}\quad,\quad(2)$$

where, $n$ is the refractive index of silica, $B_i$ and $C_i$ ($i$=1, 2, 3) are Sellmeier coefficients as shown in Table 1.

### 1.2 Theoretical model of the designed fiber

The simulation is performed on the cross-section in the $x$-$y$ plane of the PCF structure as the wave propagates in the $z$ direction. The radiation through the proposed PCF is guided by the modified total internal reflection. The following equation with the magnetic field can be derived from the Maxwell equations

$$\nabla\times\left[\frac{1}{\varepsilon_r}\nabla\times\boldsymbol{H}\right]=K_0^2\mu_r\times\boldsymbol{H}\quad,\quad(3)$$

where, $\boldsymbol{H}$ is the magnetic field strength, $\varepsilon_r$ and $u_r$ are the relative dielectric permittivity and magnetic permeability, respectively. $K_0=2\pi/\lambda$ is the wave number in vacuum. The magnetic field strength of the modal solution can be expressed as

$$\boldsymbol{H}=\boldsymbol{h}(x,y)\exp(-\mathrm{j}\beta z)\quad,\quad(4)$$

where, $\boldsymbol{h}(x,y)$ is the field distribution on the transverse plane, j is the symbol of imaginary component, $\beta=n_{\mathrm{eff}}K_0$ is the propagation constant, $n_{\mathrm{eff}}$ is the effective refractive index. The following equation with the electric field can be also derived from the Maxwell equations.

$$\nabla\times\left[\frac{1}{\mu_r}\nabla\times\boldsymbol{E}\right]=\left(\frac{\omega}{c}\right)^2\varepsilon_r\times\boldsymbol{E}\quad,\quad(5)$$

where, $\boldsymbol{E}$ is the electric field strength, c=3×10$^8$ m/s refers to the speed of light in vacuum, $\omega$ is the angular frequency of light in a vacuum. Therefore, the electric field strength can be obtained by the above method.

By solving Eqs. (3)-(5), effective refractive index ($n_{\mathrm{eff}}$), propagation constant ($\beta$), as well as magnetic field strength ($\boldsymbol{H}$) and electric field strength ($\boldsymbol{E}$) of the model can be obtained. Furthermore, birefringence ($B$), confinement loss ($L_c$) and relativity sensitivity ($r$) of the PCF can be calculated.

## 2 Numerical analysis

For the PCF designed in this paper, changing the values of $a_1$ and $b_1$ has great effects on its optical properties. Therefore, we systematically analyze the structure with different values of $a_1$ and $b_1$ when wavelength ranging from 1.2 μm to 1.8 μm. Due to the limitation of structure, the values of $a_1$ and $b_1$ cannot be too large. However, if the parameters are too small, it will be difficult to fabricate the structure. Therefore, this paper analyzes the properties of the PCF with the range of $a_1$ from 0.4 μm to 0.7 μm and the range of $b_1$ from 0.3 μm to 0.5 μm under the condition that other parameters are consistent with Section 1.1. We not only discuss the influence of $a_1$ and $b_1$ on relative sensitivity at constant temperature (20 ℃), but also analyze V-parameter, birefringence and confinement loss to ensure the practicality of the proposed PCF, because the existence of higher-order modes will bring interference in the monitoring of chemical analytes and excessive confinement loss will make the fiber useless. After comprehensively comparing the optical properties and relative sensitivity, the optimal parameters of the proposed PCF are determined.

In this work, the finite element method (FEM) is applied to solve equations of electric field and magnetic field. The PML is employed for the analysis of optical properties and the removal of leakage. The thickness of PML is 5% of the fiber radius. Fig. 2 shows the typical settings of mesh along with the boundary condition in the computed region.

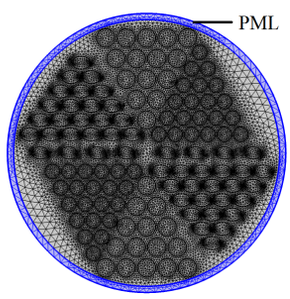


Fig. 2　Meshed model with boundary condition
图2　带有边界条件的网格模型

### 2.1 Relative sensitivity

For photonic crystal fiber, the light is mainly transmitted in the core, but there is a part of light leaking into the cladding. If the air holes in the cladding are filled with gas, liquid or other chemical analyte, the evanescent wave leaking into the air holes will be partially absorbed and results in a loss of energy. Therefore, the concentration of chemical analyte to be tested can be obtained through comparing the difference in the intensity between the output light and the incident light. Differential optical absorption spectroscopy (DOAS) is a common method used in gas or liquid sensing device. The basic principle of DOAS is that using narrow-band absorption spectrum of molecules inversion concentration of trace chemical analytes, then obtaining the concentration of the chemical analyte through the intensity of the absorption spectrum. According to the Beer-Lambert law, light is attenuated by the intensity of the evanescent wave absorption as given by [2]:

$$I(\lambda)=I_0(\lambda)\exp(-r\alpha_m lC)\quad,\quad(6)$$

where, $I(\lambda)$ represents the intensity of light with the presence of chemical analyte need to be sensed and $I_0(\lambda)$ represents the intensity without the presence of chemical analyte; $\alpha_m$ represents the absorption coefficient of the chemi-

**Table 1　Sellmeier coefficients of $SiO_2$**
**表1　$SiO_2$的Sellmeier系数**

| Coefficients | $B_1$ | $C_1$/μm$^2$ | $B_2$ | $C_2$/μm$^2$ | $B_3$ | $C_3$/μm$^2$ |
|---|---|---|---|---|---|---|
| Values | 0.6961663 | 4.679 148 26×10$^{-3}$ | 0.407 942 60 | 1.351 206 3×10$^{-2}$ | 0.897 479 40 | 97.934 002 5 |

cal analytes; $l$ represents the length of the absorbance cell and $C$ represents the concentration of the chemical analyte; $r$ represents the relative sensitivity.

From Eq. (6), it can be known that $r$ should be as high as possible to improve the sensitivity of sensing and which can be obtained from Eq. (7)[3]:

$$r = \frac{n_r}{\mathrm{Re}\left(n_{\mathrm{eff}}\right)} f \quad , \quad (7)$$

here, $n_r$ refers to the refractive index of the chemical analyte, $f$ refers to the fraction of the total power and air hole power which can be defined as[4]:

$$f = \frac{\int_{\mathrm{holes}} \mathrm{Re}\left(E_x H_y - E_y H_x\right) \mathrm{d}x\mathrm{d}y}{\int_{\mathrm{total}} \mathrm{Re}\left(E_x H_y - E_y H_x\right) \mathrm{d}x\mathrm{d}y} \quad , \quad (8)$$

here, $E_x$, $E_y$ and $H_x$, $H_y$ are the horizontal and vertical components of electric field and magnetic field respectively.

In this work, the relative sensitivity of the PCF when air holes are filled with water, ethanol and benzene is analyzed. Considering the fact that the refractive indices of ethanol and benzene will change with temperature, this work is carried out at the constant temperature of 20℃ to maintain the refractive indices of water, ethanol and benzene are 1.33, 1.354 and 1.366 respectively. When the air holes of the PCF are filled with water, ethanol or benzene, the relative sensitivity changing with wavelength are shown in Fig. 3. It can be seen that the relative sensitivity shows an upward trend as wavelength. At the wavelength of 1.55 μm, the relative sensitivities for water, ethanol and benzene all reach the maximum when $a_1$=0.7 μm and $b_1$=0.5 μm. Moreover, the PCF with $a_1$=0.7 μm and $b_1$=0.5 μm also has higher relative sensitivity than the structure with other values of $a_1$ and $b_1$ when wavelength ranging from 1.55 μm to 1.8 μm.

Fig. 4(a) shows the relative sensitivity changes with wavelength when $a_1$=0.7 μm and $b_1$=0.5 μm. At the wavelength of 1.55 μm, the relative sensitivities of this structure for water, ethanol and benzyne are 56.3%, 59.9% and 62.5%, respectively. However, the refractive indices of different chemical analytes are different. In order to further study the sensing characteristics of the structure with $a_1$=0.7 μm and $b_1$=0.5 μm, this work analyzes the relative sensitivities for other chemical analytes with refractive indices varying from 1 to 1.5. As shown in Fig. 4(b), the relative sensitivities increase with the refractive index and the relative sensitivities for chemical analytes with refractive indices varying from 1.2 to 1.4 are more affected by their intrinsic refractive indices. At the same time, as the increasing wavelength, that is, as the decreasing frequency, the relative sensitivity also tends to increase. Thus, it also has the potential for the sensing of chemicals analytes with high refractive index.

Moreover, in order to check the reliability of the results, the convergence test of this model is done. The relative sensitivities of the PCF are analyzed when the mesh is predefined as coarse, normal, fine, finer, extra fine and extremely fine. The PCF is split into 19818, 29094, 28874, 56492, 63988 and 148758 elements by the coarse, normal, fine, finer, extra fine and extremely fine mesh respectively. Fig. 5 indicates the relative sensitivity of the PCF with $a_1$=0.7 μm and $b_1$=0.5 μm changes with the degree of mesh refinement at the wavelength of 1.55 μm. It can be seen the relative sensitivity tends to be a stable value as the degree of mesh refinement. Considering the complexity of simulation and the reliability of the results, the finer mesh is employed in this work. In addition, the maximum mesh element size of the adopted mesh size is 0.503 μm, which is 503/1800 to 503/1200 of the wavelength. Therefore, the maximum mesh element size of the adopted mesh has limited to a fraction of the wavelength so that the gradient variation in the results can be analyzed accurately enough.

It is also important to optimize the PML thickness, which mainly affects the effective refractive index of PCF. According to the existing PCFs used to chemical

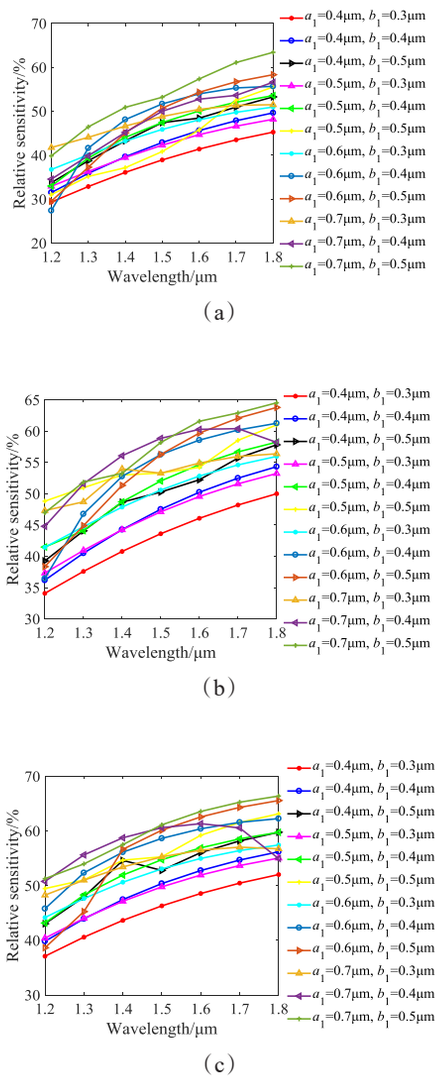


Fig. 3 Relative sensitivity for (a) water (b) ethanol (c) benzyne as a function of wavelength
图3 (a)水(b)乙醇(c)苯的相对灵敏度随波长的变化

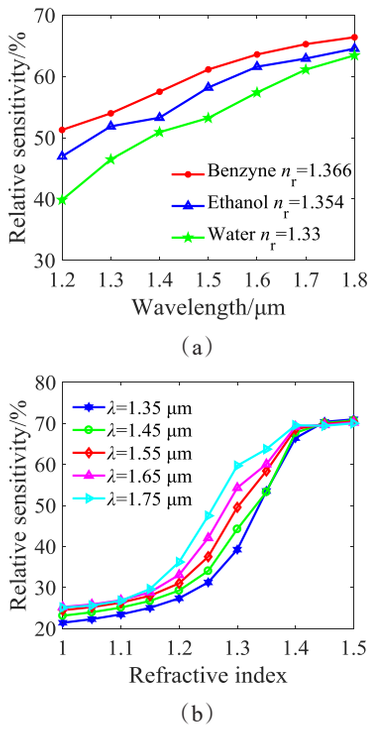


Fig. 4　Relative sensitivity as a function of (a) wavelength (b) refractive index for water, ethanol and benzyne when $a_1$=0.7 μm, $b_1$=0.5 μm

图4　$a_1$=0.7 μm, $b_1$=0.5 μm时，相对灵敏度与(a)波长(b)化学分析物的折射率的关系

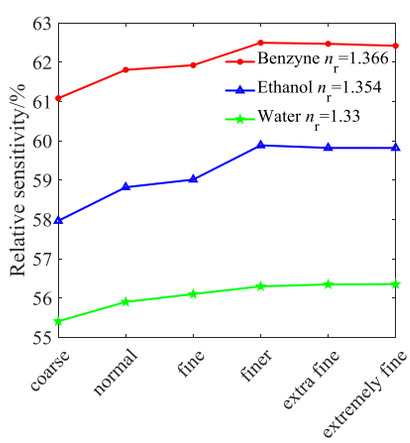


Fig. 5　Change of the relative sensitivity of the PCF with the degree of mesh refinement

图5　该PCF的相对灵敏度与网格细化程度的关系

sensor [2, 18-22], the thickness of PML is set to 5%, 10% or 20% of the fiber radius generally. Therefore, keeping all other parameters constant, we did the convergent test to choose the PML thickness, which is shown in Fig. 6. It can be seen from Fig. 6 that the variation of the real component of effective refractive index with respect to PML thickness can be negligible. As relative sensitivity is dependent on the real component of effective refractive index, thus the change of PML thickness does not affect the variation in relative sensitivity. However, the imaginary component of effective refractive index changing with PML thickness affects the confinement loss as confinement loss is dependent on the imaginary component of effective refractive index. It can be seen from Fig. 6 that the change of the imaginary component of effective refractive index is so slightly that it can be negligible. Thus, the thickness of PML has no obvious influence on the properties of the PCF, which is set to be 5% of the fiber radius in this work after considering the complexity of simulation.

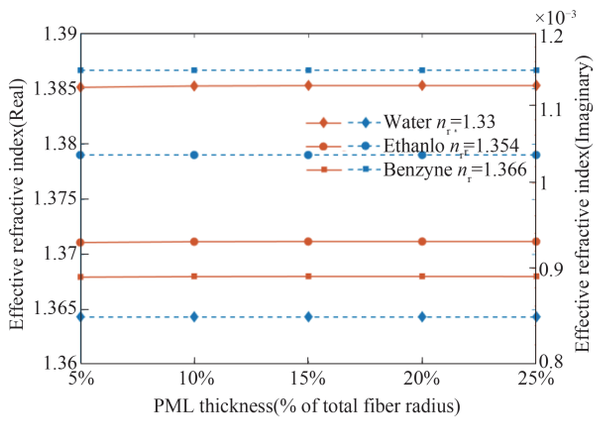


Fig. 6　Variation of effective refractive index with respect to PML variation

图6　有效折射率与PML厚度的关系

Table 2 indicates the relative sensitivities of the structure with $a_1$=0.7 μm, $b_1$=0.5 μm at typical wavelengths. As is known, in 2017, Asaduzzaman [22] *et al.* proposed a chemical sensor where core region is designed with an array of elliptical holes, the highest relative sensitivity for ethanol is 29.25% at the wavelength of 1.5 μm. Arif [23] *et al.* achieved the relative sensitivities for water and ethanol are 33% and 43.84% at the wavelength of 1.33 μm through introducing elliptical air holes in PCF. In 2019, a sensor based on PCF designed by Das [24] *et al.* obtained the relative sensitivities for water, ethanol and benzyne are below 54%, 57% and 61% at the wavelength of 1.55 μm, respectively. In 2021, Jayed [11] *et al.* designed a PCF with the hexagonal configuration of circular air holes in the cladding region, the sensitivity for water is about 40% at the wavelength of 1.55 μm. It can be seen compared with the existing PCFs [1-4, 23-25], the relative sensitivities for water, ethanol and benzyne are increased by 1.05~6.25 times, 1.05~4.99 times and 1.03~4.63 times respectively. Accordingly, the sensing accuracy will be improved. Therefore, the PCF with $a_1$=0.7 μm, $b_1$=0.5 μm has great potential in chemical sensing devices, which also can be used extremely in area of bio-sensing studies.

## 2.2　V-parameter

The existence of higher-order modes will bring interference with the monitoring of chemical analytes. So, it is necessary to analyze the single-mode property of optical fiber used in chemical sensing devices. The number of guided modes in optical fiber is determined by the val-

**Table 2 Relative sensitivity for chemical analytes at typical wavelengths**

**表2 化学分析物在典型波长下的相对灵敏度**

| Wavelength/μm | Relative sensitivity/% | | |
|---|---|---|---|
| | Water | Ethanol | Benzyne |
| 1.3 | 46.5% | 51.9% | 54% |
| 1.33 | 41.5% | 53.5% | 53.4% |
| 1.5 | 53.2% | 57.2% | 61.1% |
| 1.55 | 56.3% | 59.9% | 62.5% |

ue of $V_{\text{eff}}$. The condition of single-mode transmission for PCF is as follows:

$$V_{\text{eff}} = \frac{2\pi\Lambda}{\lambda}\sqrt{n_{\text{core}}^2 - n_{\text{eff}}^2} < 2.404\,8 \quad , \quad (9)$$

here, $n_{\text{core}}$ refers to the refractive index of core.

As shown in Fig. 7, the values of $V_{\text{eff}}$ decrease as wavelength when air holes of PCF are filled with water, ethanol and benzene respectively. Moreover, all the values of $V_{\text{eff}}$ are lower than 2.404 8, that is, the proposed PCF with different values of $a_1$ and $b_1$ has single-mode characteristic. The interference brought by high-order modes is effectively avoided when detecting the chemical analytes.

## 2.3 Birefringence

PCF with the high birefringence can eliminate the polarization modal dispersion, preserve the polarization state of the input wave and improve the stability of optical devices for sensing and improve sensing performance [25]. Therefore, the polarization maintaining property of PCF is investigated in this section.

Fig. 8 indicates refractive index of two orthogonal polarization states as a function of wavelength when $a_1$ and $b_1$ are set to different values. As can be seen, refractive indices increase with $b_1$ when $a_1$ takes a fixed value; refractive indices decrease with $a_1$ when $b_1$ takes a fixed value. At the same time, effective refractive indices of different structures decrease with the wavelength.

According to Fig. 8 and Eq. (1), we can obtain the change of birefringence with the wavelength, which is shown in Fig. 9. It can be seen from Fig. 10(a) that the birefringence increases with $b_1$ when $a_1$ is set to a fixed value at the wavelength of 1.55 μm, then reaching its maximum value when $b_1$=0.5 μm. This is because the larger the duty cycle is, the larger the difference between $\beta_x$ and $\beta_y$ becomes and the larger the difference between effective refractive indices of $x$-pol and $y$-pol becomes. Meanwhile, the birefringence increases with $a_1$ when $b_1$ is set to a fixed value at the wavelength of 1.55 μm, then reaching its maximum value when $a_1$= 0.7 μm, as shown in Fig. 10 (b). This is because the larger the ellipticity is, the higher the asymmetry of the PCF is, resulting in a larger difference in refractive index between $x$-pol and $y$-pol.

In the PCF with $a_1$=0.7 μm and $b_1$=0.5 μm, the effective refractive indices of 1.255 75 and 1.223 42 (of $x$-pol and $y$-pol) are observed at the wavelength of 1.55 μm. From Eq. (1), the birefringence of the proposed PCF is $3.233\times10^{-2}$, it is two orders for magnitude higher than traditional polarization maintaining fiber (generally

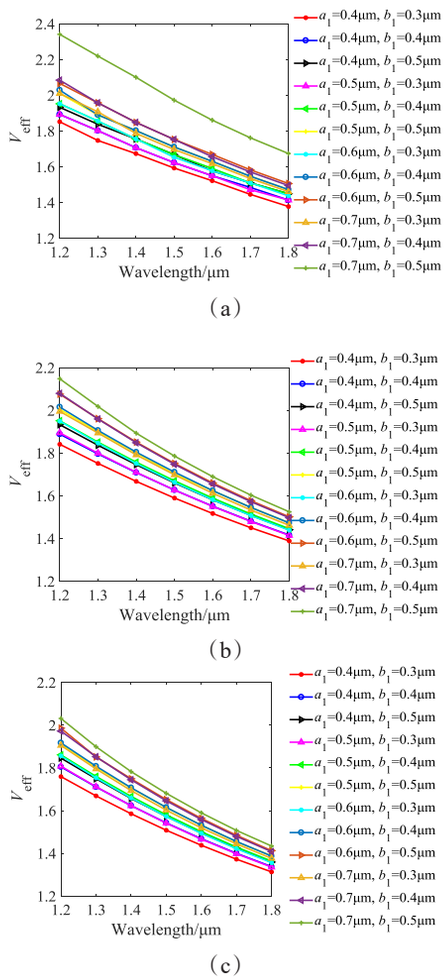


Fig. 7 The values of $V_{\text{eff}}$ for (a) water, (b) ethanol, (c) benzyne as a function of wavelength

图7 (a)水,(b)乙醇,(c)苯的$V_{\text{eff}}$随波长的变化

on the order of $10^{-4}$), and one order of magnitude higher than the existing PCFs [5, 6]. Therefore, the proposed PCF with the high birefringence conducts the sensing signal to propagate with better polarization for a long distance and provides important value for optical fiber sensing [26, 27].

## 2.4 Confinement loss

Due to the special structure of PCF, it has a kind of loss different from conventional optical fibers, that is, the confinement loss. Since the confinement loss affects the transmission distance of sensing system, it is essential to be optimized and can be calculated by the following equation:

$$L_c = \frac{20}{\ln(10)}\frac{2\pi}{\lambda}\text{Im}\left(n_{\text{eff}}\right) \quad , \quad (10)$$

where $\text{Im}(n_{\text{eff}})$ is the imaginary component of effective refractive index, representing the loss of light energy.

The change of confinement loss of the designed PCF with the wavelength is revealed in Fig. 11. With the increase in wavelength, the special structure of the PCF weakens the force of restricting light and results in the increasing confinement loss. As can be seen from Fig. 12, at the wavelength of 1.55 μm, the smaller $a_1$ or $b_1$ is, the

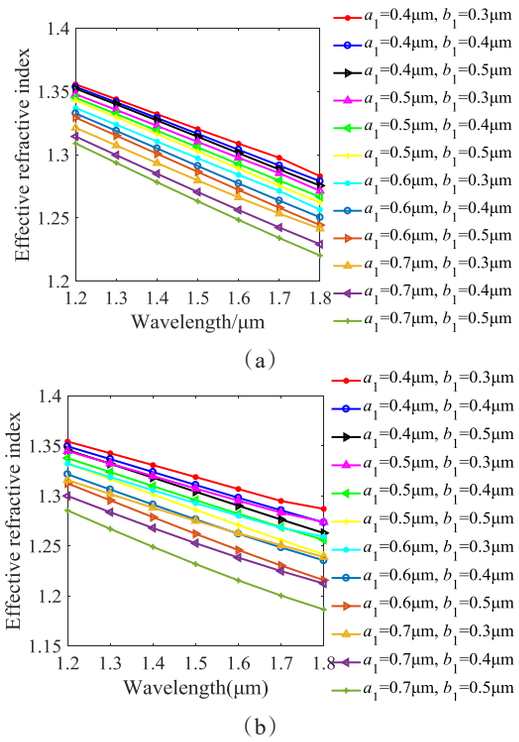


Fig. 8　Refractive index of different structures as a function of wavelength (a) *x*-pol, (b) *y*-pol

图 8　不同结构的有效折射率随波长的变化(a) *x* 轴，(b) *y* 轴

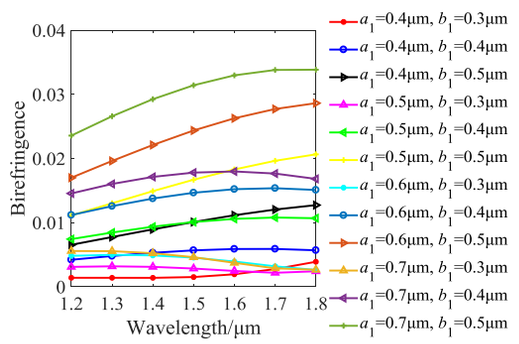


Fig. 9　Birefringence of different structures as a function of wavelength

图 9　不同结构的双折射随波长的变化

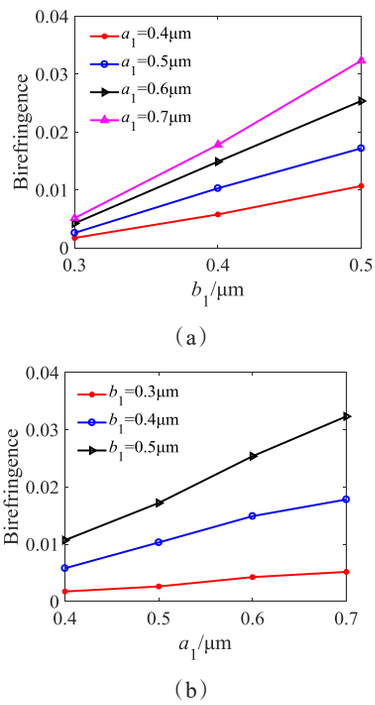


Fig. 10　Birefringence (a) when $b_1$ is set to a fixed value, (b) when $a_1$ is set to a fixed value

图 10　双折射(a) $b_1$取固定值，(b) $a_1$取固定值

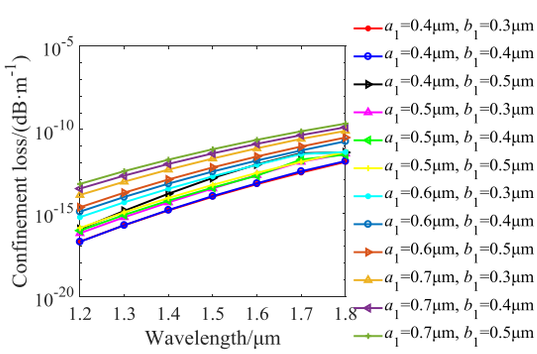


Fig. 11　Confinement loss of different structures as a function of wavelength

图 11　不同结构的限制性损耗随波长的变化

stronger the force of confinement on light energy of PCF is and the lower the confinement loss is. In addition, the influence of $a_1$ on the confinement loss is greater than the influence of $b_1$, which is because the change of $a_1$ has a greater influence on the asymmetry of the fiber cross-section.

Fig. 13 indicates the energy distribution in the core of the PCF structures with different $a_1$ and $b_1$=0.5 μm at the wavelength of 1.55 μm. It can be seen more intuitively that the confinement loss increases with $a_1$ and the energy leaks more from the core to the cladding. At the wavelength of 1.55 μm, the lowest confinement loss is on the order of $10^{-14}$ dB/m, the highest confinement loss is on the order of $10^{-11}$ dB/m. Compared with other PCFs [6, 8], the confinement loss of this PCF decreases by more than four orders for magnitude. Therefore, the reported model offering lower confinement loss can better confine the light energy inside the core. It is more conducive to the long-distance and stable propagation of the optical signal in the sensing system and is very worthy for efficient sensing.

## 2.5　Optimal structure

Considering the properties of the designed PCF mentioned in Sections 2.1~2.4, Table 3 shows the relative sensitivity, birefringence and confinement loss of the proposed PCF with different parameters at the wavelength of 1.55 μm. From Table 3, we can obtain that the optimal structure for chemical sensing takes $a_1$=0.7 μm and $b_1$=0.5 μm, which has the largest birefringence and largest relative sensitivity. Although the confinement loss of this structure is not the lowest, which is so low that the light energy can be well confined inside the core. Thus, the optimal structure has the largest birefringence, low con-

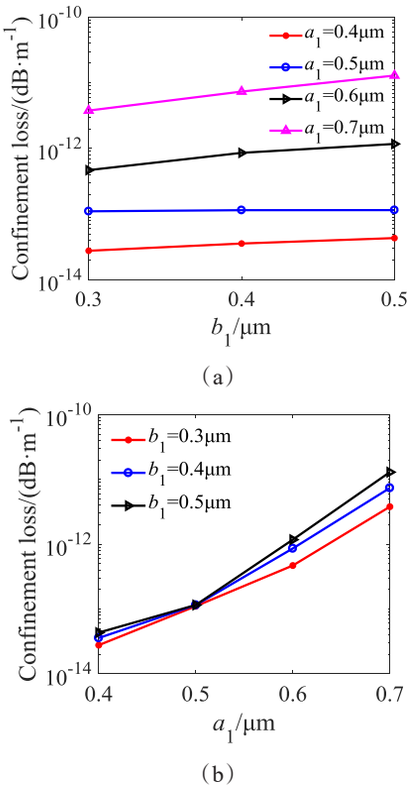


Fig. 12 Confinement loss (a) when $b_1$ is set to a fixed value, (b) when $a_1$ is set to a fixed value
图12 限制性损耗(a) b1取固定值,(b) a1取固定值

finement loss and largest relative sensitivity. The above properties are $3.233\times10^{-2}$, $1.294\times10^{-11}$ dB/m and 56.3% (water), 59.9% (ethanol), 62.5% (benzyne), respectively.

Table 4 indicates the comparison of some key properties between the optimal structure of the proposed PCF and some existing PCFs. From Table 4, we can know that the designed PCF has higher relative sensitivity for water, ethanol and benzene compared with the existing PCFs, which makes its sensing accuracy higher. At the same time, the proposed PCF has higher birefringence and lower confinement loss, which ensures that the PCF can transmit optical signals accurately and stably. Therefore, the optimal structure of this PCF has important significance in the applications of chemical sensing, environmental monitoring and biomedical field.

## 3 Feasibility of fabrication

With the rapid development of fabrication and manufacturing technology, the methods of stack and draw, 3D printing, sol-gel [28-31] have reached a very high level. It can be seen from Fig. 1 that the proposed PCF contains circular and elliptical air holes, the design and fabrication of circular air hole are common. Although the fabrication of elliptical air holes is difficult, there are many works have already achieved. For example, in 2004, Issa *et al.* [32] fabricated a PCF containing elliptical air holes which are similar in size to those in this paper and demonstrated a technique which can overcome the difficulties of heating and pressure in the stretching of fiber and the collapse sensitivity of elliptical air holes. Actually, PCFs with more complex structure than the designed PCF or similar air holes size have been fabricated [33, 34]. In addition, the proposed PCF can be fabricated easily through the method of sol-gel proposed by Hamzaoui *et al.* [31] in 2012, which can fabricate any kind of PCF structure with freedom to organize pitch, size and shape of air holes.

The proposed PCF is feasibly to be fabricated by employing the existing manufacturing technologies of PCF. Here, we only introduce a possible fabrication scheme based on the known methods. The first step of the fabrication consists in the synthesis of a cylindrical rod by the sol-gel route [31]. Then, the preform hole pattern shown in Fig. 1 is drilled into extruded preform, this is subsequently drawn to a structured cane. The obtained rod is integrated into an air/silica PCF structure using the conventional stack-and-draw process to obtain the circular air holes. A technique employing hole deformation during optical fiber draw can be adopted for the fabrication of PCF with uniformly oriented elliptical holes [30]. Thirdly, Porous silica monoliths, shaped as cylinders, are prepared from tetraethyl ortho silicate (TEOS). Some of those porous monoliths exhibiting interconnected nanometer pores, which is doped by soaking it into a copper salt solution. Later, the sample is taken out and dried for several hours to remove solvents. At last, the resulting xerogel is densified under air atmosphere at 1200 °C. In this way, the PCF is obtained. The way of pressurizing UV-curable polymer inside the PCF can be used to selectively fill the PCF air holes with liquid analytes [9].

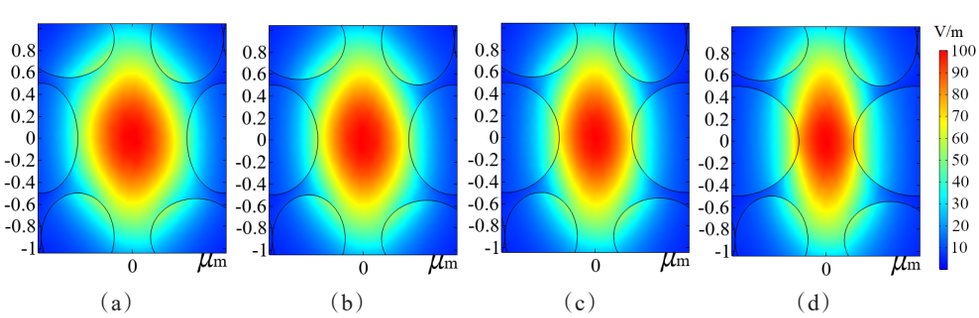


Fig. 13 The energy distribution of the fiber core when $b_1$=0.5 μm and (a) $a_1$=0.4 μm, (b) $a_1$=0.5 μm, (c) $a_1$=0.6 μm, (d) $a_1$=0.7 μm
图13 b1=0.5 μm且(a) a1=0.4 μm, (b) a1=0.5 μm, (c) a1=0.6 μm, (d) a1=0.7 μm时纤芯的能量分布

**Table 3 The properties of PCF with different structures**
**表3 不同结构的光子晶体光纤的特性**

| Parameter/μm | Relative sensitivity/% | | | Birefringence | Confinement loss/(dB·m$^{-1}$) |
|---|---|---|---|---|---|
| | Water | Ethanol | Benzyne | | |
| $a_1$=0.4, $b_1$=0.3 | 40.1 | 44.8 | 47.4 | $1.732\times10^{-3}$ | $2.765\times10^{-14}$ |
| $a_1$=0.4, $b_1$=0.4 | 44.3 | 48.9 | 51.6 | $5.79\times10^{-3}$ | $3.565\times10^{-14}$ |
| $a_1$=0.4, $b_1$=0.5 | 47.9 | 51.2 | 54.4 | $1.07\times10^{-2}$ | $4.319\times10^{-14}$ |
| $a_1$=0.5, $b_1$=0.3 | 43.5 | 48.3 | 50.8 | $2.61\times10^{-3}$ | $1.105\times10^{-13}$ |
| $a_1$=0.5, $b_1$=0.4 | 48.8 | 53.3 | 55.8 | $1.03\times10^{-2}$ | $1.149\times10^{-13}$ |
| $a_1$=0.5, $b_1$=0.5 | 43.3 | 53.8 | 57.2 | $1.72\times10^{-2}$ | $1.152\times10^{-13}$ |
| $a_1$=0.6, $b_1$=0.3 | 47 | 51.7 | 54 | $4.244\times10^{-3}$ | $4.685\times10^{-13}$ |
| $a_1$=0.6, $b_1$=0.4 | 52.8 | 47.4 | 59.5 | $1.49\times10^{-2}$ | $8.595\times10^{-13}$ |
| $a_1$=0.6, $b_1$=0.5 | 52.5 | 57.9 | 61.3 | $2.537\times10^{-2}$ | $1.175\times10^{-12}$ |
| $a_1$=0.7, $b_1$=0.3 | 49.6 | 54.1 | 55.8 | $5.161\times10^{-3}$ | $3.789\times10^{-12}$ |
| $a_1$=0.7, $b_1$=0.4 | 51.3 | 59.6 | 60.9 | $1.781\times10^{-2}$ | $7.376\times10^{-12}$ |
| $a_1$=0.7, $b_1$=0.5 | 56.3 | 59.9 | 62.5 | $3.233\times10^{-2}$ | $1.294\times10^{-11}$ |

**Table 4 Comparison of properties of different PCFs**
**表4 不同光子晶体光纤的特性比较**

| Ref. | Wavelength/μm | Relative sensitivity/% | | | Birefringence | Confinement loss/(dB·m$^{-1}$) |
|---|---|---|---|---|---|---|
| | | Water | Ethanol | Benzyne | | |
| [1] | 1.5 | 9 | 12 | 13.5 | $10^{-3}$ | $10^{-1}$ |
| [17] | 1.5 | — | 29.5 | — | — | $7.68\times10^{-7}$ |
| [22] | 1.33 | 33 | 43.84 | — | $2.83\times10^{-3}$ | $2.07\times10^{-6}$ |
| [23] | 1.55 | <54 | <57 | <61 | — | $2.26\times10^{-3}$ |
| [10] | 1.3 | 49.13 | — | — | $8\times10^{-3}$ | $5.583\times10^{-5}$ |
| [10] | 1.55 | 46 | — | — | — | — |
| [12] | 1.55 | 40 | — | — | $3.1\times10^{-3}$ | — |
| Proposed PCF | 1.55 | 56.3 | 59.9 | 62.5 | $3.23\times10^{-2}$ | $1.294\times10^{-11}$ |

## 4 Conclusion

A novel PCF used for chemical sensing is proposed in this work, in which air holes are arranged in the triangular lattice. The arrangement of air holes in cladding is diagonally symmetrical. The optimal structure is obtained by numerical calculation and analysis. At the wavelength of 1.55 μm, the relative sensitivities for water, ethanol and benzyne of the PCF with the optimal structure are up to 56.3%, 59.9% and 62.5%, respectively. Compared with the existing PCFs, they are improved by 1.05~6.25 times, 1.05~4.99 times and 1.03~4.63 times, respectively. At the same time, the birefringence and confinement loss of the optimal structure are $3.233\times10^{-2}$ and $1.294\times10^{-11}$ dB/m respectively. Compared with the existing PCFs, they are improved by one order for magnitude and decreased by 4 orders for magnitude, respectively. Therefore, the proposed PCF provides a new method for obtaining chemical sensor with the high birefringence and low confinement loss. It is expected to show excellent performance in chemical sensing, industrial chemical research and biomedical fields.

## Acknowledgement

This work was supported by the National Natural Science Foundation of China (Grant Nos. 61775057, 62171185), the Natural Science Foundation of Hebei Province, China (Grant Nos. E2020502010, E2019502177), the Fundamental Research Funds for the Central Universities (Grant No. 2019MS085, 2021MS072), S & T Program of Hebei (SZX2020034).

## Explanation to the innovation

In this work, a novel photonic crystal fiber (PCF) with high birefringence and low confinement loss is designed, which can be used for sensing of chemical analytes. Different from the axisymmetric structure used in existing PCFs, the proposed PCF is designed to be diagonally symmetrical, which increase the asymmetry of PCF and improve its properties further. The results show that the relative sensitivities of the optimal structure for water, ethanol and benzene at wavelength of 1.55 μm are 56.3%, 59.9% and 62.5%, respectively. Compared with the existing PCFs, the relative sensitivities are improved by 1.05~6.25 times, 1.05~4.99 times and 1.03~4.63 times, respectively. At the same time, the birefringence and confinement loss of the optimal structure are $3.233\times10^{-2}$ and $1.294\times10^{-11}$ dB/m at the wavelength of 1.55 μm, respectively. Compared with exist-

ing PCFs, they are improved by one order for magnitude and decreased by 4 orders for magnitude, respectively.

## References


[1] Ademgil H, Haxha S. Highly Birefringent Nonlinear PCF for Optical Sensing of Analytes in Aqueous Solutions [J]. *Optik-International Journal for Light and Electron Optics*, 2016, **127**(16): 6653-6660.

[2] Islam M S ,Sultana J, Rifat A A, *et al*. Terahertz Sensing in a Hollow Core Photonic Crystal Fiber[J]. *IEEE Sensors Journal*, 2018: 1-1.

[3] Zhao L J, Zhao H Y, Xu Z N. Design of High-sensitivity Hydrostatic Pressure Sensor Based on Brillouin Dynamic Grating [J]. *Acta Photonica Sinica*,(赵丽娟, 赵海英, 徐志钮. 基于布里渊动态光栅的高灵敏度静压力传感器设计. **光子学报**) 2021, **50**(2): 29-44.

[4] Saitoh K, Koshiba M. Leakage Loss and Group Velocity Dispersion in Air-core Photonic Bandgap Fibers[J]. *Optics Express*, 2003, **11**(23): 3100-3109.

[5] Liu M, Hou J, Yang X, *et al*. Design of Photonic Crystal Fiber with Elliptical Air-holes to Achieve Simultaneous High Birefringence and Nonlinearity[J]. *Chinese Physics B*, 2018, **27**(1): 014206.

[6] Saha R, Hossain M M, Rahaman M E, *et al*. Design and Analysis of High Birefringence and Nonlinearity with Small Confinement Loss Photonic Crystal Fiber [J]. *Frontiers of Optoelectronics*, 2019, **11**(42): 315-418.

[7] Paul B K, Rajesh E, Asaduzzaman S, *et al*. Design and Analysis of Slotted Core Photonic Crystal Fiber for Gas Sensing Application[J]. *Results in Physics*, 2018, **11**: 643-650.

[8] Rabee A S H, Hameed M F O, Heikal A M, *et al*. Highly Sensitive Photonic Crystal Fiber Gas Sensor [J]. *Optik*, 2019, **188**: 78-86.

[9] Malavika R, Prabu K. Design Optimization of a Highly Sensitive Spiral Photonic Crystal Fiber for Liquid and Chemical Sensing Applications[J]. *Optical fiber technology*, 2019, **51**(1): 36-40.

[10] Leon M J B M, Kabir M A. Design of a Liquid Sensing Photonic Crystal Fiber with High Sensitivity, Bireferingence & Low Confinement Loss[J]. *Sensing and Bio-Sensing Research*, 2020, 28.

[11] Leon M J B M, Abedin S, Kabir M A. A Photonic Crystal Fiber for Liquid Sensing Application with High Sensitivity, Birefringence and Low Confinement Loss[J]. *Sensors International*, 2020, 2.

[12] Olyaee S, Naraghi A, Ahmadi V. High Sensitivity Evanescent-field Gas Sensor Based on Modified Photonic Crystal Fiber for Gas Condensate and Air Pollution Monitoring[J]. *Optik-International Journal for Light and Electron Optics*, 2014, **125**(1): 596-600.

[13] Hou S, Lei J, Wu Q. Enhanced Femtosecond Optical Pulses Compression in Highly Nonlinear Photonic Crystal Fibers[J]. *Infrared Laser Engineering*, (侯尚林, 雷景丽, 吴七灵, 等. 高非线性光子晶体光纤中飞秒脉冲压缩. **红外与激光工程**) 2019,**48**(1): 58-63.

[14] Musideke M, Yao J Q, Lu Y R, et al, Highly Nonlinear and Birefringent Photonic Crystal Fiber at 1.55μm[J]. *Optics and Precision Engineering*, (马依拉木·木斯得克, 姚建铨, 陆颖,等. 1.55 μm高非线性高双折射光子晶体光纤. **光学精密工程**) 2014, **22**(3): 588-596.

[15] Wang E L, Jiang H M, Xie K, *et al*. Photonic Crystal Fiber with High Birefringence and High Nonlinearity and Multiple Zero-dispersion Wavelengths[J]. *Acta Physica Sinica*, (王二垒, 姜海明, 谢康, 等. 一种高双折射高非线性多零色散波长光子晶体光纤. **物理学报**) 2014, **63**(13): 199-204.

[16] Yang T Y, Jiang H M, Wang E L, *et al*. Photonic Crystal Fibers with Large Birefringence and High Nonlinearity in Near-infrared Band [J]. *Journal of Infrared and Millimeter Waves*, (杨天宇, 姜海明, 王二垒, 等. 一种近红外波段的高双折射高非线性光子晶体光纤. **红外与毫米波学报**) 2016, **35**(3): 350-354.

[17] Wei W, Zhang Z M, Tang L Q, *et al*. Transmission Characteristics of Vortex Beams in A Sixfold photonic Quasi-crystal Fiber[J]. *Acta Physica Sinica*, (魏薇, 张志明, 唐莉勤, 等. 六重准晶涡旋光光子晶体光纤特性. **物理学报**) 2019, **68**(11): 179-185.

[18] Paul B K, Islam M S, Ahmed K, *et al*. Alcohol Sensing over O+E+S+C+L+U Transmission Band Based on Porous Cored Octagonal Photonic Crystal Fiber[J]. *Photonic Sensors*, 2017, **7**(2): 123 - 130.

[19] Mu'iz M A, Yakasai I, Abas P E, *et al*. Design and Simulation of Photonic Crystal Fiber for Liquid Sensing[J]. *Photonics*, 2021, **8**(1): 16.

[20] Yang T, Zhang L, Shi Y, *et al*. A Highly Birefringent Photonic Crystal Fiber for Terahertz Spectroscopic Chemical Sensing[J]. *Sensors*, 2021, **21**(5): 1799.

[21] Arif M, Biddut M. A New Structure of Photonic Crystal Fiber with High Sensitivity, High Nonlinearity, High Birefringence and Low Confinement Loss for Liquid Analyte Sensing Applications[J]. *Sensing and Bio-Sensing Research*, 2017, **12**(C): 8-14.

[22] Ahmed K, Asaduzzaman S. Microarray-core Based Circular Photonic Crystal Fiber for High Chemical Sensing Capacity with Low Confinement Loss[J]. *Optica Applicata*, 2017, **47**(1): 41-49.

[23] Arif M, Bidut M, Enhancement of Relative Sensitivity of Photonic Crystal Fiber with High Birefringence and Low Confinement Loss[J]. *Optik*, 2017, **131**: 697-704.

[24] Das S, De M, Singh V K. Single Mode Dispersion Shifted Photonic Crystal Fiber with Liquid Core for Optofluidic Applications[J]. *Optical Fiber Technology*, 2019, **53**: 102012.

[25] Emiliyanov G, Høiby P E, Pedersen L H, *et al*. Selective Serial Multi-Antibody Biosensing with TOPAS Microstructured Polymer Optical Fibers[J]. *Sensors*, 2013, **13**(3): 3242-3251.

[26] Pang M. Birefringence of Hybrid PCF and Its Sensitivity to Strain and Temperature[J]. *Journal of Lightwave Technology*, 2012, **30**(10): 1422-1432.

[27] Xu Z N, Hu Y H, Zhao L J, *et al*. Fast and Highly Accurate Brillouin Frequency Shift Extracted Algorithm Based on Modified Quadratic Polynomial fit[J]. *Spectroscopy and Spectral Analysis*, (徐志钮, 胡宇航, 赵丽娟, 等. 基于改进二次多项式拟合的布里渊频移快速高精度提取算法,**光谱学与光谱分析**) 2020, **40**(03): 842-848.

[28] Ghazanfari A, Li W, Leu M C, *et al*. A Novel Freeform Extrusion Fabrication Process for Producing Solid Ceramic Components with Uniform Layered Radiation Drying [J]. *Additive Manufacturing*, 2017, **15**: 102-112.

[29] Cubillas A M, Unterkofler S, Euser T G, *et al*. Photonic Crystal Fibres for Chemical Sensing and Photochemistry[J]. *Chemical Society Reviews*, 2013, 42 22.

[30] Ebendorff-Heidepriem H, Schuppich J, Dowler A, *et al*. 3D-printed Extrusion Dies: A Versatile Approach to Optical Material Processing[J]. *Optical Materials Express*, 2014, **4**(8): 1494-1504.

[31] Hamzaoui H E, Ouerdane Y, Bigot L, *et al*. Sol-gel Derived Ionic Copper-doped Microstructured Optical Fiber: A Potential Selective Ultraviolet Radiation Dosimeter[J]. *Optics Express*, 2012, **20**(28): 29751-29760.

[32] Issa N A, Eijkelenborg M, Fellew M, *et al*. Fabrication and Study of Microstructured Optical Fibers with Elliptical Holes[J]. *Optics Letters*, 2004, **29**(12): 1336-1338.

[33] Bise R T, Trevor D J. Sol-gel Derived Microstructured Fiber: Fabrication and Characterization[C]. Optical Fiber Communication Conference, 2005. Technical Digest. OFC/NFOEC. IEEE, 2005.

[34] Jewart C M, Sully Mejía Quintero, Braga A M B, *et al*. Design of A Highly-birefringent Microstructured Photonic Crystal Fiber for Pressure Monitoring[J]. *Optics Express*, 2010, **18**(25): 25657.